Stability of Electrostatic Actuated Membrane Mirror Devices

Peter Kurczynski and Bernard Sadoulet

University of California, Berkeley and

Bell Laboratories, Lucent Technologies

Abstract

Membrane mirrors with transparent electrodes were fabricated for adaptive optics. These devices are capable of large, low order deformations but exhibit instability for high order deformations. A variational calculation of the electrostatic and mechanical energy of such membrane devices leads to criteria for stable operation. Simulations based upon this calculation are able to reproduce the observed behavior of a fabricated device and suggest suitable device parameters for improved performance of high order deformations.

41.20.Cv, 42.65.Sf, 42.79.-e, 46.70.Hg

1. Introduction

Membrane deformable mirrors have been used as wavefront correctors for adaptive optics.[1] Micro-electromechanical systems (MEMS) technology enabled the fabrication of low-stroke membrane mirrors that have been used in a wide variety of applications.[2] Recently, the need for wavefront deformations on the order of 10 μm for correction of aberrations in vision science and other adaptive optics applications motivated the fabrication of devices made from low stress silicon membranes; these devices are capable of larger deformations than have previously been reported in membrane mirrors.[3]

These devices consist of a grounded, conducting membrane suspended over an electrode array, which deforms the membrane via electrostatic actuation. Electrostatic pressure exerted on the membrane via underlying, charged electrodes pulls the membrane toward this underlying electrode plane. Due to the pull-in nature of the electrostatic attraction, only the membrane tension can provide an opposing force to deform the membrane in the opposite direction. This tension is insufficient to generate enough upward deformation for the correction of many optical distortions, with typical device geometries and material parameters. An opposing, electrostatic restoring force to the membrane was provided by the use of an additional electrode plane that consisted of a transparent electrode that is positioned in the optical path, above the membrane. This technique was previously utilized in a macro-machined membrane mirror.[4] The transparent electrode acts as a bias electrode that can in principle greatly increase the range of membrane deformation.

Due to the relatively small membrane-electrode spacing, and low material stress, the device is observed to be stable only within a limited range of operating voltages. Instability arises from increasing the electrostatic pressure on both sides of the membrane, as the electrode voltages are increased; instability manifests as membrane snap-down toward either electrode plane. This paper presents an analysis of the stability of the membrane as a function of various device parameters, and concludes with device parameters necessary to yield stable operation at large membrane deformation.

2. Method

The static equilibrium of the membrane may be analyzed by considering variations of the total electrostatic plus mechanical energy of the device. The electrostatic contribution to the energy is found by integration of the electric field over the volume of the device. The mechanical energy is expressed as an integral over the membrane surface. A variational method is used, whereby the first variation of the energy yields the equation of equilibrium and the second variation of the energy is used to analyze the stability of an arbitrary membrane configuration.

The equation of static equilibrium of the membrane is derived in Section 3.1. Eigenfunctions of the membrane, which are useful for later calculations, are derived in Section 3.2. The second variation of the energy is calculated in Section 3.3, and this result is used to derive a criterion for small amplitude deformations in Section 3.4. Treatment of the more general case of large deformations leads to a matrix diagonalization problem, and eigenvalue analysis, discussed in Section 3.5. Implementation of the matrix diagonalization method to simulate device performance is covered in Section 4. Section 5 discusses results of these simulations and Section 6 presents data from a laboratory device for comparison with the simulations.

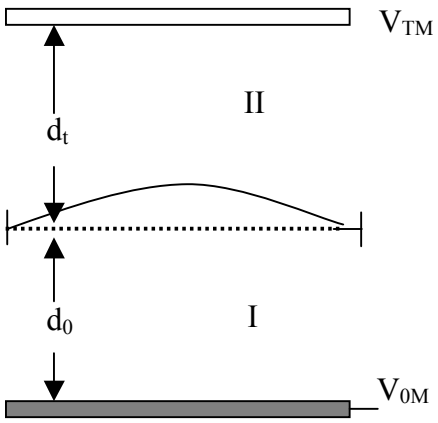

Figure 1. Schematic diagram of a membrane mirror device. The membrane, solid line, is located between top, transparent electrode and bottom, actuating electrode. The membrane experiences deformations relative to the flat position (dashed line) in response to electric fields in regions I and II. Voltages refer to the relative voltage between the respective electrode plane and the membrane, which may be at ground or at some non-zero voltage.

3. Analysis

3.1. Equation of equilibrium.

The equation of equilibrium is found by expressing the total electrostatic plus mechanical energy as an integral and demanding this integral be stationary with respect to arbitrary deformations of the membrane.

The electrostatic contribution to the energy is minimized when the membrane snaps down to one or the other electrode plane. In the absence of material tension, a symmetric device* under voltage would have an unstable equilibrium when the membrane is flat. Any small deformation toward either electrode results in a net electrostatic force pulling the membrane toward the closer electrode plane.

The electrostatic energy, U_{el}, is found from integrating the volume energy density of the electrostatic field, E, on either side of the membrane, i.e. region I and region II defined in Figure 1. This quantity, expressed as an integral over the volume of regions I and II, is given as

$$U_{el} = \int \frac{1}{2} \varepsilon_0 E_I^{\,2} dV_I + \int \frac{1}{2} \varepsilon_0 E_{II}^{\,2} dV_{II} \tag{1}$$

For electrode planes at uniform voltages, V_T and V_A, and membrane at voltage V_M, such that the relative voltages are defined as V_{TM} and V_{AM}, electric fields are given by

$$E_I = \frac{V_{TM}}{(d_T + \xi)} \tag{2}$$

$$E_{II} = \frac{V_{AM}}{(d_0 - \xi)} \tag{3}$$

Below, the membrane will be considered at ground and the absolute voltages used. Integration over the vertical dimension in Figure 1 can be carried out to yield an expression in terms of the integral over the membrane surface

---

* A symmetric device is defined as one in which gap distances and voltages on each electrode plane are equal.

$$U_{el} = \frac{\varepsilon_0}{2}\int \frac{V_A^2}{d_A - \xi} dS + \frac{\varepsilon_0}{2}\int \frac{V_T^2}{d_T + \xi} dS \tag{4}$$

For the case of an array of discrete electrodes underneath the membrane, each of area Δs_k, the first term on the right hand side becomes

$$\int \frac{\varepsilon_0 V_A^2}{2\left(d_A - \xi\right)} dS \Rightarrow \frac{\varepsilon_0}{2}\sum_k \frac{V_k^2}{d_A - \xi_k}\Delta s_k \tag{5}$$

and the energy is expressed as a sum over the individual electrodes

$$U_{el} = \frac{\varepsilon_0}{2}\sum_k \frac{V_k^2}{d_A - \xi_k}\Delta s_k + \frac{\varepsilon_0}{2}\int \frac{V_T^2}{d_T + \xi} dS \tag{6}$$

This case will be considered explicitly in Section 4. For the remainder of this Section, a uniform voltage, V_a, will be assumed on all electrodes of the array and the integral expression given in Equation (4) will be used.

The mechanical contribution to the energy is found by considering the tension in the membrane, which acts parallel to the surface of the membrane. This tension acts as a restoring force to the membrane that prevents electrostatic induced snap down for suitably small deformations. Tension acts to pull the membrane flat, and increasing the tension makes the membrane harder to deform for a given set of voltages applied to the electrodes.

The mechanical contribution to the energy is given by

$$U_{me} = \frac{1}{2}\int T\left(\nabla\xi\right)^2 dS \tag{7}$$

This expression ignores the effects of bending stress; prior simulations have demonstrated that bending stress is a small fraction of the material stress (e.g. 10% for low stress membranes) for deformations that are typical of adaptive optics mirrors.

The total energy, $U = U_{el} + U_{me}$, is given by combining Equations (4) and (7)

$$U = \int\left[\frac{\varepsilon_0}{2}\frac{V_A^2}{d_A - \xi} + \frac{\varepsilon_0}{2}\frac{V_T^2}{d_T + \xi} + \frac{1}{2}T\left(\nabla\xi\right)^2\right]dS \tag{8}$$

For the membrane to be in static equilibrium, the total energy must be stationary with respect to arbitrary variations, δξ, of the membrane shape function.

The variation in the total energy is given by

$$\delta U = U\left(\xi + \delta\xi\right) - U\left(\xi\right) \tag{9}$$

where

$$U\left(\xi + \delta\xi\right) = \int\left[\frac{\varepsilon_0}{2}\frac{V_A^2}{d_A - \xi + \delta\xi} + \frac{\varepsilon_0}{2}\frac{V_T^2}{d_T + \xi + \delta\xi} + \frac{1}{2}T\nabla\left(\xi + \delta\xi\right)\cdot\nabla\left(\xi + \delta\xi\right)\right]dS \tag{10}$$

The first two terms of the integrand in Equation (10) can be expanded as a Taylor series in powers of $\delta\xi$, retaining only terms up to $O\left(\delta\xi\right)$. The third term of the integrand in Equation (10) can be multiplied out, also retaining terms up to $O\left(\delta\xi\right)$, and integrated by parts (surface term vanishes because $\delta\xi=0$ at the membrane boundary). After subtracting

the energy $U(\xi)$, given by Equation (8), these simplifications yield an integral expression for the energy variational

$$\delta U = \int \left[-T\nabla^2\xi - \frac{1}{2}\varepsilon_0 \frac{V_A^2}{\left(d_A - \xi\right)^2} + \frac{1}{2}\varepsilon_0 \frac{V_T^2}{\left(d_T + \xi\right)^2} \right] \delta\xi dS \tag{11}$$

The condition for equilibrium consists of this integral being an extremum, $\delta U=0$, which for arbitrary variations $\delta\xi$ requires the quantity in [] to be zero. This requirement leads to the equation of equilibrium for the membrane

$$T\nabla^2\xi = -\frac{\varepsilon_0 V_A^2}{2\left(d_A - \xi\right)^2} + \frac{\varepsilon_0 V_T^2}{2\left(d_T + \xi\right)^2} \tag{12}$$

Stability of the equilibrium can be analyzed by taking a second variation, $\delta^2 U$ starting from Equation (11). This computation, carried out in Section 3.3 is complicated by the presence of ∇^2 in the integrand of Equation (11). Expansion of the membrane variation, $\delta\xi$, in eigenfunctions of the ∇^2 operator, which are computed in the next section, will allow expression of $\delta^2 U$ in terms of these eigenfunctions. The resulting energy variational will be found as a matrix, whose eigenvalues will be used to determine the stability of equilibrium.

3.2. Eigenfunctions of the membrane.

Given a membrane, of radius a, the eigenfunctions, ζ_{vn}, and eigenvalues, λ_{vn}, satisfy the equation

$$\nabla^2 \xi_{vn} = -\lambda_{vn}{}^2 \xi_{vn} \tag{13}$$

subject to the boundary condition that the membrane have zero deformation at its periphery, i.e. $\xi_{vn}\left(r = a\right) \Rightarrow 0$. The eigenfunctions are labeled with two integer indices, *v,n*, in anticipation of the solution in two dimensions. Equation (13) can be solved in polar coordinates using separation of variables to yield the eigenvalues, which are the separation constants

$$\lambda_{vn} = \frac{x_{vn}}{a} \tag{14}$$

where x_{vn} is the n'th zero of Bessel function $J_v(\rho)$. Eigenfunctions are given by

$$\xi_{vn} = \frac{1}{a\sqrt{\pi}\left|J_{v+1}\left(x_{vn}\right)\right|} J_v\left(x_{vn}\frac{\rho}{a}\right) e^{iv\phi} \tag{15}$$

These eigenfunctions satisfy the orthonormality condition

$$\int \xi_{vn}\bar{\xi}_{v'n'} dS = \delta_{vv'}\delta_{nn'} \tag{16}$$

where δ denotes a Kronecker delta, $\bar{\xi}_{v'n'}$ is the complex conjugate of $\xi_{v'n'}$, and integration is over the membrane surface. Representative eigenfunctions are illustrated in Figure 2. Subsequently in this paper, eigenfunctions will be labeled by a single index, j, which combines both v and n.[a]

---

[a] In simulations described below, this j index is related to the natural indices by j=9v+n-1. The simulations generate 53 membrane eigenfunctions, and perform matrix calculations on this basis.

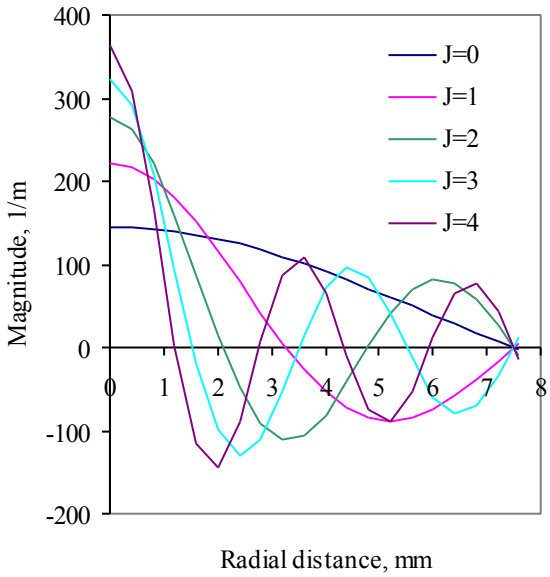

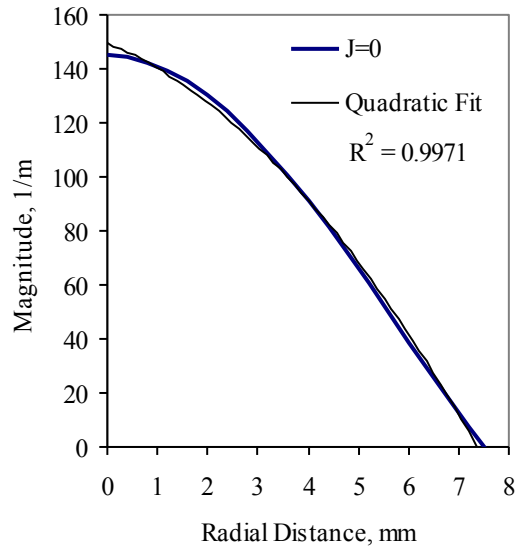

Figure 2 a,b Representative eigenfunctions for a 7.5 mm radius membrane. Each plot graphs the magnitude of the complex eigenfunction, m^{-1} vs. radial coordinate, mm. Left figure (a) illustrates the first 5 eigenfunctions, indexed by j value, where j=9v+n-1. Each eigenfunction has j+1 nodes in the interval [0,5]. Right figure (b) illustrates the zero'th order eigenfunction and a quadratic fit. The lowest eigenfunction is very nearly a parabola.

3. Second variation of the energy function.

An understanding of the stability of the membrane will follow from an analysis of the second variation of the energy function. In order to complete the calculation, this energy functional will be expressed in terms of the eigenfunctions of the membrane. This expression will lead to a small amplitude approximation and a criterion for stability, given in Section 3.4, and a matrix expression for the more general case of large amplitude stability, discussed in Section 3.5

The first variation of the combined electrostatic and mechanical energy, Equation (11), is given by

$$\delta U = \int \left[-T\nabla^2 \xi - \frac{1}{2}\varepsilon_0 \frac{V_A^2}{\left(d_A - \xi\right)^2} + \frac{1}{2}\varepsilon_0 \frac{V_T^2}{\left(d_T + \xi\right)^2} \right] \delta\xi dS \tag{17}$$

The second variation is found by differentiation

$$\delta^2 U = \int \left[-T\nabla^2 \left(\delta\xi\right) - \frac{\varepsilon_0 V_A^2}{\left(d_A - \xi\right)^3}\delta\xi - \frac{\varepsilon_0 V_T^2}{\left(d_T + \xi\right)^3}\delta\xi \right] \delta\xi dS \tag{18}$$

The second and third terms of the integrand, involving electrostatic quantities, can be combined into a single "weight function"

$$\Im(\xi) \equiv \frac{\varepsilon_0 V_A^2}{\left(d_A - \xi\right)^3} + \frac{\varepsilon_0 V_T^2}{\left(d_T + \xi\right)^3} \tag{19}$$

Thus the second variation of the energy is composed of a tension term and an electrostatic term.

$$\delta^2 U = -\int T\nabla^2\left(\delta\xi\right)\delta\xi dS - \int \Im(\xi)\delta\xi dS \equiv \delta^2 U_A + \delta^2 U_B \tag{20}$$

Expanding the variation of the membrane shape in terms of the membrane eigenfunctions will permit further simplification.

$$\delta\xi = \sum_{vn} b^{vn}\xi_{vn} \tag{21}$$

Taking the complex conjugate of Equation (21), and using the fact that $\delta\xi$ is real gives

$$\delta\xi = \sum_{vn} \bar{b}^{vn}\bar{\xi}_{vn} \tag{22}$$

Inserting the above expansions into the expression for $\delta^2 U_A$ gives

$$\delta^2 U_A = \int\left[-T\nabla^2\left(\sum_{vn} b^{vn}\xi_{vn}\right)\sum_{v'n} \bar{b}^{v'n'}\bar{\xi}_{v'n'}\right]dS \tag{23}$$

Equation (23) can be further simplified using the eigenvalue equation for the basis functions, ξ_{vn},

$$\nabla^2\xi_{vn} = -\left(\frac{x_{vn}}{a}\right)^2 \xi_{vn} \tag{24}$$

Using Equation (24) to evaluate the Laplacian in Equation (23) leads to

$$\delta^2 U_A = \int\left[T\left(\sum_{vn} b^{vn}\left(\frac{x_{vn}}{a}\right)^2 \xi_{vn}\right)\sum_{v'n} \bar{b}^{v'n'}\bar{\xi}_{v'n'}\right]dS \tag{25}$$

$$\delta^2 U_A = T\sum_{v,v'n,n'}\left(\frac{x_{vn}}{a}\right)^2 b^{vn}\bar{b}^{v'n'}\int\xi_{vn}\bar{\xi}_{v'n'}dS \tag{26}$$

Finally, orthonormality of the basis functions, ξ_{vn}, given by Equation (16), is used compute the integral

$$\delta^2 U_A = T \sum_{\nu,\nu' n,n'} \left(\frac{x_{\nu n}}{a} \right)^2 b^{\nu n} \bar{b}^{\nu' n'} \delta_{\nu\nu'} \delta_{nn'} \tag{27}$$

$$\delta^2 U_A = T \sum_{\nu,n} \left(\frac{x_{\nu n}}{a} \right)^2 b^{\nu n} \bar{b}^{\nu n} \tag{28}$$

The second term in the equation for the second variation of the energy, Equation (20), can also be simplified using the expansions in terms of the membrane eigenfunctions given by Equations (21) and (22):

$$\delta^2 U_B = -\int \Im(\xi) \sum_{\nu,n} b^{\nu n} \zeta_{\nu n} \sum_{\nu',n'} \bar{b}^{\nu' n'} \bar{\zeta}_{\nu' n'} dS \tag{29}$$

These expressions for the second variation of the energy, given by Equations (28) and (29) can be used to investigate the stability behavior of a membrane device under a variety of conditions and device parameters. A stable device configuration has $\delta^2 U > 0$. A criterion for stability is obtained for small amplitude deformations in Section 3.4. The more general case of large amplitude deformations is treated in Section 3.5.

3.4. Small deviations from flat membrane.

For the special case of $\Im \equiv \Im_0$, a constant, (i.e. ξ independent of ρ,φ, and in particular when ξ=0), this constant can be moved outside the integral of Equation (29).

$$\delta^2 U_B = -\Im_0 \sum_{\nu,n} b^{\nu n} \sum_{\nu',n'} \bar{b}^{\nu' n'} \int \zeta_{\nu n} \bar{\zeta}_{\nu' n'} dS \tag{30}$$

Orthonormality of the eigenfunctions can be used to compute the integral in Equation (30)

$$\delta^2 U_B = -\Im_0 \sum_{v,n} b^{vn} \sum_{v',n'} \bar{b}^{v'n'} \delta_{vv'} \delta_{nn'} \tag{31}$$

$$\delta^2 U_B = -\Im_0 \sum_{v,n} b^{vn} \bar{b}^{vn} \tag{32}$$

Equation (32) is combined with Equation (28) above to yield an expression for the complete second variation of the energy function, $\delta^2 U$, for the special case $\Im \equiv \Im_0$, a constant, including when ξ=0

$$\delta^2 U = \sum_{v,n} T\left(\frac{x_{vn}}{a}\right)^2 b^{vn} \bar{b}^{vn} - \Im_0 \sum_{v,n} b^{vn} \bar{b}^{vn} \tag{33}$$

$$\delta^2 U = \sum_{v,n} \left[T\left(\frac{x_{vn}}{a}\right)^2 - \Im_0 \right] b^{vn} \bar{b}^{vn} \tag{34}$$

Equation (34) is used to derive a criterion for stability appropriate for small amplitude deformations. For these deformations, $\zeta \approx 0$ and the assumption of constant $\Im$ is approximately correct. A stable equilibrium implies $\delta^2 U > 0$, which condition requires the term in square brackets to be positive for all values of *v,n*.

$$T\left(\frac{x_{vn}}{a}\right)^2 - \Im_0 > 0 \tag{35}$$

Substituting the value of $\Im_0 \left(\xi = 0\right)$ into the above equation leads to the expression

$$T\left(\frac{x_{vn}}{a}\right)^2 - \left(\frac{\varepsilon_0 V_A^2}{d_A^{\,3}} + \frac{\varepsilon_0 V_T^2}{d_T^{\,3}}\right) > 0 \tag{36}$$

The inequality in Equation (36) is a difference of two terms that are always positive. The lowest values of the quantities x_{vn} are illustrated in Table 1. Substituting the minimum value for x_{vn} leads to the requirement

$$\left(\frac{\varepsilon_0 V_A^2}{d_A^{\,3}} + \frac{\varepsilon_0 V_T^2}{d_T^{\,3}}\right) < T\left(\frac{x_{01}}{a}\right)^2 \tag{37}$$

This expression indicates that, for maximum stability of the un-deformed membrane, voltages on the array and the transparent electrode, V_A and V_T, should be minimized, while the gap distances, d_A and d_T, should be maximized.

For the case of a symmetric device, where gap distances are equal, $d_A = d_T \equiv d$, Equation (29) describes a circular region in voltage space bounded by a critical radius, r_V.

$$r_V \equiv \frac{x_{01}}{a}\sqrt{\frac{Td^3}{\varepsilon_0}} \tag{38}$$

$$V_A^2 + V_T^2 < r_V^2 \tag{39}$$

Figure 3 illustrates this parameter space for typical parameters of a transparent electrode membrane device. Gap distances were 30 μm; membrane stress was 3 MPa, radius was 7.5 mm and thickness was 1.0 μm. The thick solid curve in Figure 3 illustrates the

radius, r_V. The shaded region of the figure is the region of stability computed by the more general, large amplitude stability computation, discussed below, with membrane deformation pinned to zero; this region is practically indistinguishable from the small amplitude analytic result of Equation (39), and serves to validate the large amplitude stability computation. Only the region of parameter space near the diagonal in Figure 3 is self-consistent; elsewhere the combined voltages would induce large amplitude deformations in violation of the assumption of small amplitude deformation inherent in Equation (39).

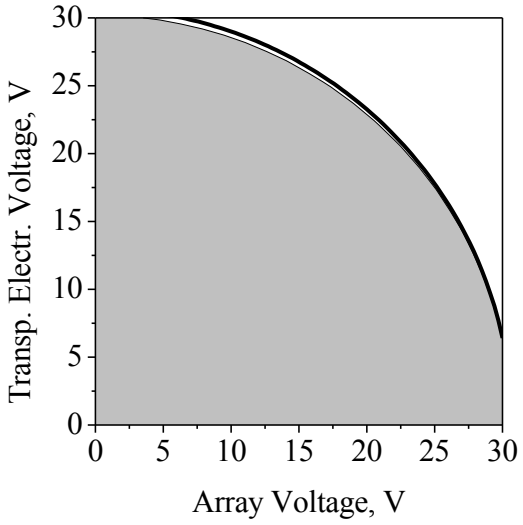

Figure 3. Stability diagram for simulated small amplitude deformations of a membrane device. Shading indicates the parameter space corresponding to stable small amplitude deformations. Contour plot obtained from eigenvalue analysis of simulated device. Thick line coincident with the edge of the shaded contour indicates the corresponding analytic approximation of the limit of stability.[b]

[b] Figure from …/Formal Stability Calculation/Data/04-18-2005/Small Amplitude Deformation Expt/(origin plot). Copy…paste into MS Word.

x_{vn}, n'th zero of Bessel function J_v.	value
x_{01}	2.405
x_{11}	3.832
x_{21}	5.136
x_{02}	5.520
x_{12}	7.016

Table 1. Zeros of Bessel functions J_v

3.5. General case of large deflections: diagonalization of the stability matrix

In the more general case of arbitrary deflections of the membrane, the function $\Im(\xi)$ cannot be moved outside the integral in Equation (29). This general case can be reduced to a matrix expression for $\delta^2 U$; diagonalization of this matrix and inspection of its eigenvalues leads to a sufficient condition for stability of the membrane.

The double summations in Equation (29) can be re-written as single summations by defining new indices j, j' where each value of the new index corresponds to a unique combination of v, n etc.

$$\delta^2 U_B = -\int \Im(\xi) \sum_j b^j \zeta_j \sum_{j'} \bar{b}^{j'} \bar{\zeta}_{j'} dS \tag{40}$$

Moving the summations and the expansion coefficients, b^j , $\bar{b}^{j'}$, outside the integral and rewriting the integral as a matrix element gives

$$\delta^2 U_B = -\sum_{j,j'} b^j \bar{b}^{j'} A_{jj'} \tag{41}$$

The matrix element element is defined

$$A_{jj'} \equiv \int \Im(\xi) \zeta_j \bar{\zeta}_{j'} dS \tag{42}$$

Similarly, re-writing the summation in Equation (28) in terms of the new indices j, j' gives

$$\delta^2 U_A = T \sum_j \left(\frac{x_j}{a} \right)^2 b^j \bar{b}^j \tag{43}$$

Anticipating combining this expression with the corresponding expression for $\delta^2 U_B$, Equation (43) can be written in terms of a double sum over j, j' as

$$\delta^2 U_A = \sum_{j,j'} T \left(\frac{x_j}{a} \right)^2 b^j \bar{b}^{j'} \delta_{jj'} \tag{44}$$

where $\delta_{jj'}$ is a kronecker delta.

The two components of $\delta^2 U$ can be combined to give

$$\delta^2 U = T\sum_{j,j'}\left(\frac{x_j}{a}\right)^2 b^j \bar{b}^{j'}\delta_{jj'} - \sum_{j,j'} b^j \bar{b}^{j'} A_{jj'} \tag{45}$$

$$\delta^2 U = \sum_{J,J}\left[T\left(\frac{x_j}{a}\right)^2 \delta_{jj'} - A_{jj'}\right] b^j \bar{b}^{j'} \tag{46}$$

The quantity in square brackets can be represented as a Hermitian matrix:

$$\Omega \equiv \begin{pmatrix} T\left(\frac{x_1}{a}\right)^2 - A_{11} & & -A_{1M} \\ & & \\ -A_{M1} & & T\left(\frac{x_M}{a}\right)^2 - A_{MM} \end{pmatrix} \tag{47}$$

The dimension, M, of this matrix spans all of the V*N basis functions used in the expansions of Equations (28) and (29). This matrix, Ω, can be diagonalized by a similarity transformation, whereby the resulting diagonal entries of the matrix are its eigenvalues, λ_j. Operating on Equation (46) with this similarity transformation leads to an equivalent expression for $\delta^2 U$ as the sum of the product of these eigenvalues with the norms of the expansion coefficients b^j.

$$\delta^2 U = \sum_{j=1}^{M} \lambda_j \left\| b^j \right\|^2 \tag{48}$$

Requiring that the equilibrium be stable imposes the condition $\delta^2 U > 0$. Because the norms of the expansion coefficients are non-negative, a sufficient condition for stability is therefore that all of the eigenvalues, λ_j, be non-negative.

In subsequent simulations, analysis of the eigenvalues, λ_j, will be used to determine the stability characteristics of membrane devices. If the lowest eigenvalue is negative, then the simulated device configuration is unstable. When considering a range of device parameters, such as operating voltages, the range over which the lowest eigenvalue remains non-negative determines the range of stable operation of the device.

4. Device Simulation.

The procedure for diagonalizing the stability matrix outlined in Section 3.5 was implemented in software to enable the investigation of various device parameters for their stability characteristics. The simulations began with an input membrane shape function, ξ, expressed in terms of the eigenfunctions of the membrane.[c] From this membrane shape function, the self-consistent electrode voltages required to produce the given input shape function were computed, as discussed in Section 4.1. From these voltages, the matrix elements $A_{jj'}$ given by Equation (51) were computed by summing over discrete electrode pixels based upon a model of actual devices fabricated and tested in the laboratory. For comparison and validation of the code, matrix elements were also computed using the integral approximation given by Equation (42). For small deflection amplitudes and electrode voltages, these methods of computation gave similar results, as illustrated in Table 2. Finally, the stability matrix, Ω, given by Equation (47) was computed and diagonalized to yield a set of eigenvalues and eigenvectors. The

[c] An expansion into as many as 53 membrane eigenfunctions were used.

eigenvalues were used to determine stability; negative eigenvalues for a given simulation indicated an unstable device configuration. Simulations were run with varying gap distances, membrane tension and electrode voltages to identify the parameter space for stable operation and determine optimum parameters for device stability.

4.1. Electrode Voltage Computation

A self-consistent simulation of the device performance requires that the voltages, V_a, and V_t be consistent with the actual shape of the membrane, as given by Equation (12). Furthermore, the derivation has so far considered the electrode array as being energized to a single, uniform voltage, V_a, whereas in practice each electrode of the array will have a unique voltage applied to it. For a given membrane shape function, ξ, the required electrode voltages may be obtained from Equation (12) by solving for V_a. In this case the membrane shape function is evaluated at the positions of the electrode centers, i.e. $\xi_k = \xi(r_k)$, where r_k denotes the position of electrode k on the electrode plane.

$$V_k^2 = \frac{2(d_A - \xi_k)^2}{\varepsilon_0}\left[\frac{\varepsilon_0 V_T^2}{(d_T + \xi_k)^2} - T\nabla^2\xi_k\right] \tag{49}$$

The quantity in [] must be non-negative for physically realizable membrane shapes. This restriction places a lower limit on the transparent electrode voltage, V_t. Provided this lower limit is satisfied, the membrane deformation and voltages can be made self-consistent.

The corresponding electrostatic weight function, the generalization of Equation (19) is given by

$$\Im(r_k) = \varepsilon_0 \frac{V_k^2}{(d_A - \xi_k)^3} + \varepsilon_0 \frac{V_T^2}{(d_T + \xi_k)^3} \tag{50}$$

The matrix element, given by Equation (47) is computed by approximating the surface integral as a sum over the membrane surface.

$$A_{jj'} = \sum_k \Im(r_k) \xi_j(r_k) \xi_{j'}(r_k) \Delta s_k \tag{51}$$

The sum is over patches of the membrane surface that correspond to electrodes of the underlying array, as well as equally sized patches that extend from the periphery of the array to the outer edge of the membrane. These patches completely tile the membrane surface.[d]

5. Results of Simulation

5.1. Range of stable device operation.

Simulations of devices with a transparent electrode indicate that stable operation of the devices depends upon judicious choice of membrane-electrode gap distances and operating voltages. In a device with a transparent electrode, the membrane is pulled from both sides by the opposing electrodes. This competition of forces leads to instability. In general, larger gap distance devices can operate over a wider range of deformations than

[d] In calculations below, the sum consisted of 2916 terms, corresponding to a 54x54 grid.

smaller gap distance devices. However, large deformations require high transparent electrode voltages, which limit the domain of stability for a given device.

Increasing the membrane tension (stress x thickness) also increases stability; however highly tensile membranes require larger voltages to generate a given deformation. The simulations discussed below use a membrane tension of 3 N/m, corresponding to 3 MPa stress and 1 μm thickness membranes, similar to devices that have been fabricated and reported previously.

Figure 4 illustrates the eigenvalue variation as a function of peak deformation for various device configurations. Positive eigenvalues correspond to stable device configurations; negative eigenvalues correspond to unstable device configurations. These data were obtained using a J_0 Bessel function input and the computational procedure described above. The input membrane shape for these simulations was approximately parabolic, eigenfunction j=0, see Figure 2, and therefore of low spatial frequency. Higher spatial frequency deformations are considered in Section 5.2. The upper, dashed curve of Figure 4 illustrates a simulated device with 75 μm membrane-electrode array and 75 μm membrane-transparent electrode gap distances,[e] operated at 50 V transparent electrode voltage. The corresponding electrode array voltages were computed in a self-consistent manner as described in Section 4.1. This device is stable over a broad range of deflections; however, the range of deflection toward the transparent electrode,

---

[e] Devices with equal gap distances are indicated as symmetric in the figures.

corresponding to negative deformations in Figure 4, is limited to 5 μm by the operating voltage. Increasing the operating voltage in principle allows greater negative deformations, but diminishes the overall region of stability.

Devices with smaller gap distances, illustrated in Figure 4 have reduced regions of stability. The middle dashed curve corresponds to 50 μm symmetric gap distances and 40 V transparent electrode operation; the lower dashed curve corresponds to 25 μm gap distances and 20 V transparent electrode operation.

The middle, solid curve of Figure 4 illustrates the simulation of a device fabricated in the laboratory. This device has 27 μm transparent electrode-membrane gap distance and 36 μm membrane-electrode array gap distance, and the simulation indicates stable operation from –7 μm to 10 μm. Laboratory experiments with this device were able to demonstrate ±10 μm deformation, discussed further in Section 6, indicating broad agreement of the simulation with the actual device.

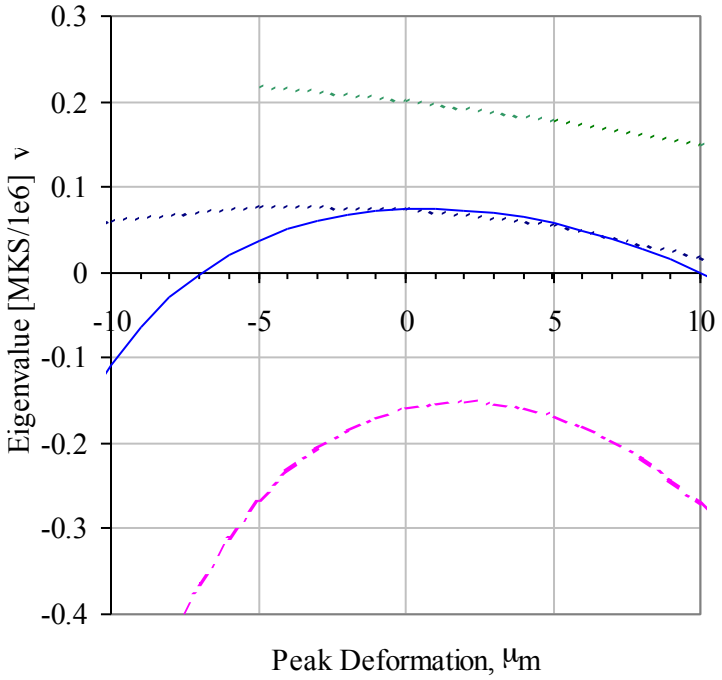

Figure 4. Lowest eigenvalue vs. peak deformation for simulated devices. Positive eigenvalues indicate regions of stable device operation. Upper (middle) [lower] dashed curves illustrate simulated devices with 75 (50) [25] μm membrane-electrode distances (symmetric). Middle, solid curve illustrates eigenvalue variation for device with asymmetrical 27/36 μm gap distances similar to a device tested in the laboratory.

Simulations indicate that devices with larger gap distances can operate with larger electrode voltages in a stable manner. Figure 5 illustrates the eigenvalues vs. transparent electrode voltage for a set of devices and membrane configurations. The upper, dashed curve of Figure 5 corresponds to a 75 μm, symmetric gap distance device, producing a membrane deformation of 10 μm peak deformation; this configuration is stable from 0-80

V. The middle, dashed curve illustrates 10 μm peak deformation produced by a device with 50 μm symmetric gap distances; this device configuration is stable from 0-40 V. The solid curve illustrates a simulation of the device tested in the laboratory, and discussed in Section 6 with 27/36 μm gap distances. This simulated device is stable at transparent electrode voltages up to 20 V. The actual device tested in the laboratory was found to become unstable with transparent electrode voltages in excess of approximately 17 V.

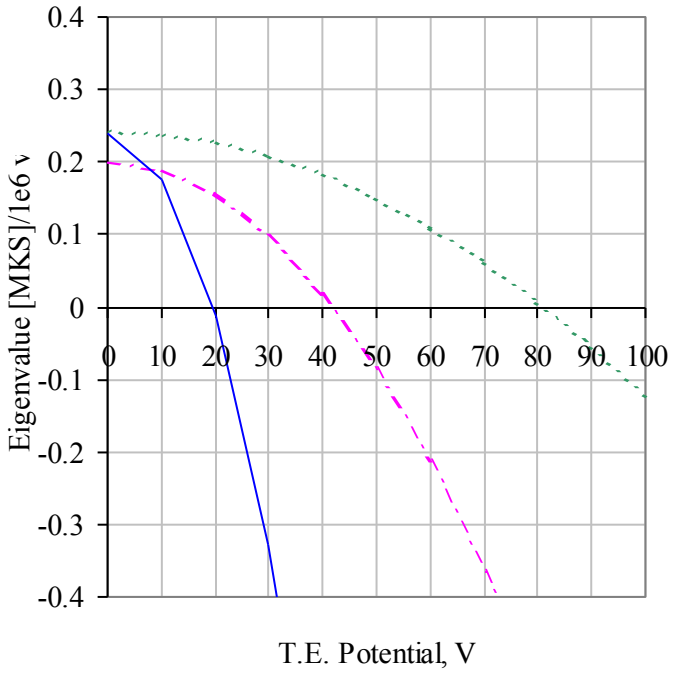

Figure 5. Eigenvalues of stability matrix vs. transparent electrode voltage for various device configurations. Positive values of the eigenvalues correspond to stable configurations. Top curve, dashed line, corresponds to a device with gap distance of 75 μm (symmetric). Middle curve, dot-dashed line, corresponds to gap

distances of 50 μm and lower curve, solid line, simulates gap distances of 27 μm for transparent electrode and 36 μm for electrode array, corresponding to a device tested in the laboratory. Devices with large gap distances are stable over a wider range of electrode voltages.

5.2. Maximum stable deformation

In general, electrostatic actuated MEMS devices become unstable and experience snap down when the actuation distance is 1/3 the gap distance between un-deformed electrodes. This result can be derived analytically for discrete, segmented electrode actuators. Simulations indicate that a more complex relationship pertains for membrane devices. Membrane devices can achieve stable deformations larger than the 1/3 gap limit for the lowest eigenmode; however they are limited to less than the 1/3 gap limit for higher spatial frequency deformations.

Figure 6 illustrates the maximum peak deformation of several membrane devices as a function of eigenmode number. The first four eigenmodes were studied in simulated devices with 30, 50, 75 μm membrane-electrode gap distances. Membrane radius was 7.5 mm, tension was 3 N/m (3 MPa stress; 1 μm thickness). Each eigenmode is a Bessel function of the radial coordinate, as illustrated in Figure 7a for the j=2 eigenmode. The voltage distribution required to produce the deformations were also computed, as illustrated in Figure 7b.

Device stability depends upon the value of the transparent electrode bias voltage, as discussed previously. The data for Figure 6 were obtained by selecting the minimum value of the bias voltage that would allow the device to produce the required deformation. This value of the bias voltage was selected by incrementally increasing the bias voltage from a small value, computing the electrode voltage distribution at each increment, and requiring that this electrode voltage distribution be entirely real. Imaginary voltages are unphysical and indicated that the bias voltage needed to be increased in order for the device to produce the required deformation.

Table 3 illustrates the maximum amplitude[f] deformation obtained for single electrode plane devices based on the eigenvalue analysis. Various membrane-electrode gap distances were simulated. The membrane tension was 3 N/m and the membrane radius was 7.5 mm. The input membrane shape was the lowest order membrane eigenfunction, j=0. The resulting peak deformation was toward the electrode plane; the value of the peak deformation was approximately 130% 1/3 gap distance for all simulations. Thus for low spatial frequency deformations, the membrane can deform to greater than the 1/3 gap distance limit normally associated with MEMS devices.

Table 4 illustrates the maximum amplitude deformation obtained for transparent electrode plane devices that are capable of deformation toward either electrode plane. Device parameters were the same as discussed above, however the membrane shape was

---

[f] Amplitude here is defined as the maximum zero to peak distance, which for the Bessel function is measured at $r=0$.

the membrane eigenfunction, j=1. This radial component of this eigenfunction has a single node midway between the membrane center and edge. The maximum amplitude of stable deformation obtained with this higher spatial frequency eigenfunction is 30-35% 1/3 gap distance. Thus the membrane cannot generate the higher spatial frequency deformations as effectively as lower spatial frequency deformations. Further simulations with j=2 and j=3 eigenfunctions support this conclusion, as illustrated in Figure 6.

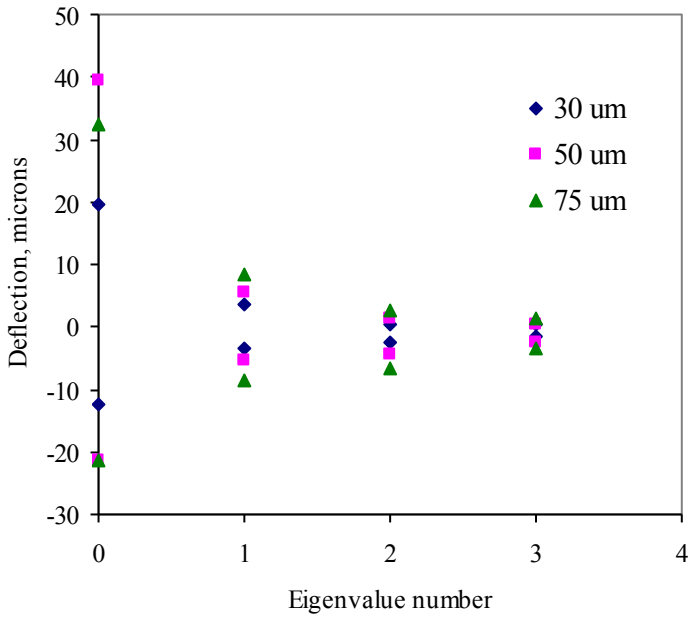

Figure 6. These data illustrate maximum, stable, peak deformation for the first four eigen-modes of the membrane device, for several different membrane-electrode gap distances. Positive deformations are toward the transparent electrode; negative deformations are toward the electrode array. Data from …/Data/06-17-2005/J1_3PeakDefVariationSummary_v2.xls

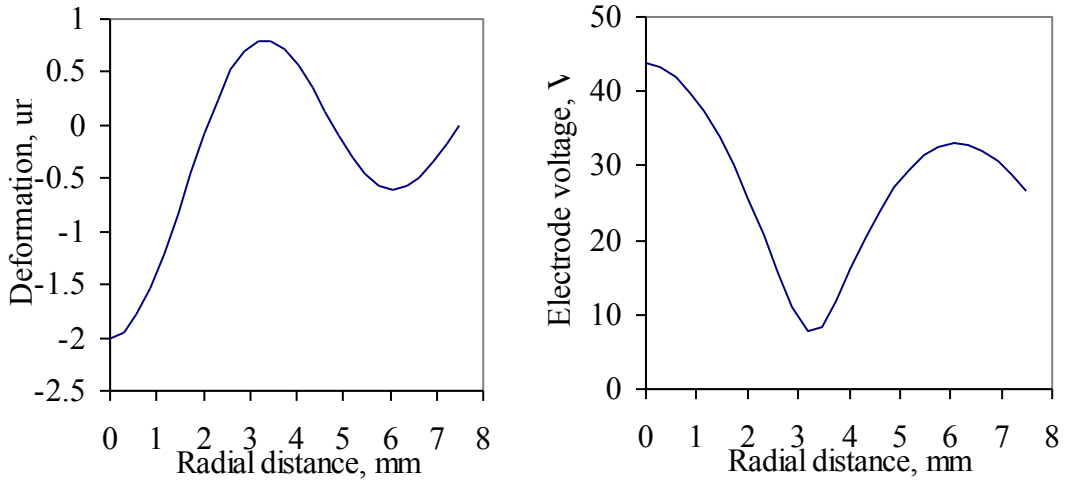

Figure 7a,b. Left figure (a) illustrates membrane shape corresponding to j=2 eigenmode. Peak deformation is toward the electrode array (negative value). Right figure (b) illustrates voltage distribution on the array necessary to produce the shape from figure (a), with a device consisting of 30 um gap distances, and 25 V transparent electrode bias voltage. Data from …/Data/06-17-2005/J_2PeakDefVariationExptDataExcerpt_v2a.xls

Gap dist	max def	1/3 gap dist	% 1/3 gap
30	13.5	10.0	135%
50	21.5	16.7	129%
75	32.5	25	130%

Table 3. Maximum stable deformation amplitude for single electrode plane devices. Input membrane shape was a membrane eigenfunction, j=0. Left column is the membrane-electrode array gap distance, in microns, for the simulated device. Second column indicates the deflection at which instability occurs based upon the large amplitude stability computation. Third column indicates the 1/3 gap distance

for the device. The last column indicates the maximum deformation distance as a percentage of the 1/3 gap distance. Data from …Data/06-20-2005/ J0_SingleElectrodePeakDefVariationExptData_v1.xls

gap dist	max def.	1/3 gap dist	% 1/3 gap	max voltage
30	3.5	10.0	35%	33
50	5.5	16.7	33%	71
75	8.5	25.0	34%	110

Table 4. Maximum stable deformation amplitude for several device configurations. Input membrane shape was a membrane eigenfunction, j=1. Peak deformation was toward the transparent electrode. First column indicates the membrane-electrode gap distance in microns. Second column indicates the maximum stable deformation, in microns, from simulations. The 1/3 gap distance in microns is indicated in the third column and the fourth column indicates the percentage of the 1/3 gap value achieved by the maximum deformation. The last column indicates the peak voltage on the array necessary to produce the deformation.

6. Experimental Results from Membrane Devices

Membrane devices were fabricated that demonstrate large amplitude (>10 μm) low order deformation consistent with the simulations discussed above. The membrane devices presented here were fabricated from 1 μm thickness SOI; details of the membrane

characteristics and fabrication were presented previously.[5] Devices were bonded to electrode arrays with 1024 electrodes, packaged in ceramic pin grid arrays and driven by off chip D/A electronics.

Transparent electrodes were placed over the membrane; they consisted of 300 μm thickness Borofloat ® glass that was ITO coated for electrical conductivity and visible light transmission. An electrode was inserted into a recessed cavity of each membrane chip, and was fixed 25-50 μm above the membrane.

Measurements of the devices were made with a Shack-Hartmann wavefront sensor from Adaptive Optics Associates; reconstructed wavefronts are illustrated below. Closed loop operation of these devices will be presented elsewhere.

The first device had gap distances of 27 μm membrane-transparent electrode, and 36 μm membrane-electrode array as measured with a Wyko interferometer

Figure 8 illustrates the optical wavefront resulting from large deformations being applied to one membrane device. These data illustrate control of the optical wavefront over a 38 μm range, corresponding to nearly 70 wavelengths. The membrane deformed by 10 μm (mechanical) deformation toward either electrode plane. The resulting deformations were stable.

Due to a fabrication defect, the membrane of the first device was tilted with respect to the electrode planes. As a result, the deformations in Figure 8 are off center with respect to

the optical pupil. This de-centration made the device difficult to control for generating arbitrary deformations. Also visible in the wavefront reconstructions of Figure 8 are circular artifacts around the edge of the pupil; these are images of vent holes in the transparent electrode; they are located outside the intended active pupil of the device.

The device exhibited stable operation at transparent electrode voltages between 0-17 V, in agreement with the results of simulations discussed in Section 5. At larger bias voltages, the device became unstable and experienced snap down toward either electrode plane.

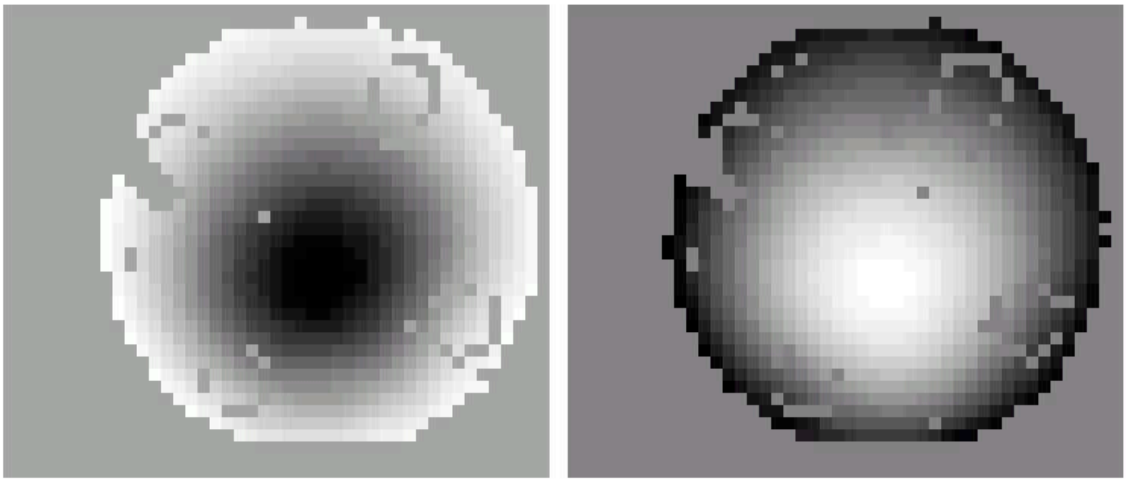

Figure 8 a,b. Wavefront optical path difference resulting from operation of device #1. Left figure (a) illustrates 20 μm PV OPD resulting from membrane deformation toward electrode array. Right figure (b) illustrates 18 μm PV OPD resulting from membrane deformation toward transparent electrode. Device 11-17-2004-A. Image 11-17-2004-A__EA_20_40um__TE_17_8um.jpg

A second membrane device, device #2 below, was fabricated using the same procedure, but with different gap distances. This device demonstrated control of the optical wavefront over a 50 μm range, corresponding to 90 wavelengths, under stable operation. A representative wavefront, 15 μm optical deformation, resulting from 30 V applied to the transparent electrode, is illustrated in Figure 9. Even greater deformations toward the transparent electrode, estimated 30 μm optical, were achieved with this device; however, measurements were limited to less than 20 μm by spot confusion in the wavefront sensor. Combined with deformations of 20 μm optical toward the electrode array, this device demonstrated a total wavefront deformation of 50 μm.

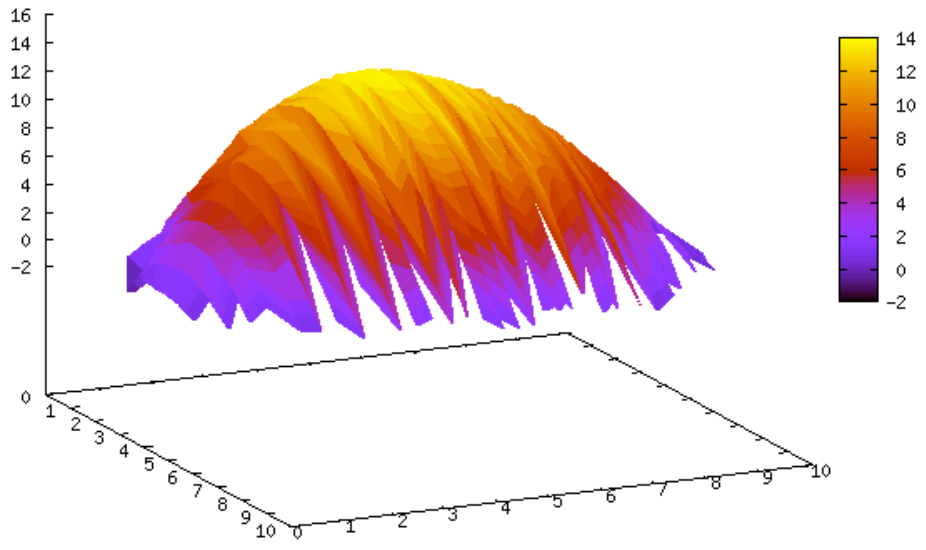

Figure 9. Wavefront optical path difference from operation of device #2. Z axis in microns, X,Y axes in mm (?). Deformation toward transparent electrode, 15 μm peak deformation. Transparent electrode voltage was 30 V.

This device had a membrane-transparent electrode distance of 56 μm and membrane-electrode array distance of 19 μm. Deflection vs. voltage data for deformation toward each electrode plane are illustrated in Figure 10.

The data in Figure 10 are compared to an analytical model of the membrane deformation that has been successful in describing the general characteristics of membrane devices in general. This model consists of a solution of the Poisson equation of equilibrium for the membrane, with the electrostatic pressure approximated to 1'st order in the membrane deformation. Parameters of the model include the gap distance between electrode plane

and membrane, membrane stress and other geometrical parameters. The membrane stress is a free parameter of the model; however previous direct measurements of similar membranes placed this value at 3-7 MPa.

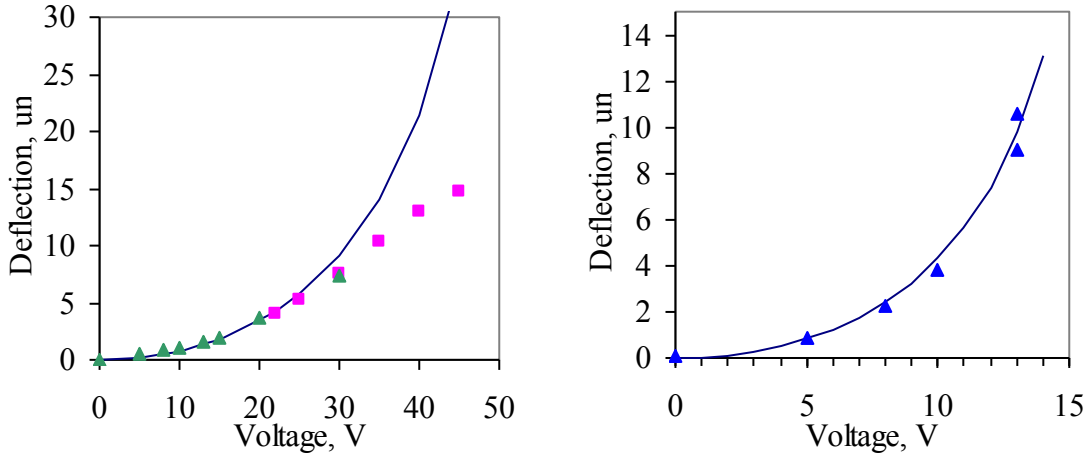

Figure 10 a,b. Mechanical membrane deflection vs. voltage data for membrane device #2. Left figure (a) illustrates deflection (in microns) toward transparent electrode as a function of transparent electrode voltage. Data for deflections greater than 10 microns are under-estimates of the actual deflection due to limitations of the wavefront sensor. Model fit (solid curve) to the small deflection data is for a 3 MPa stress membrane, 56 μm gap distance. Right figure (b) illustrates deflection (in microns) toward electrode array as a function of electrode array voltage. Model fit (solid curve) is for a 3 MPa stress membrane, 19 μm gap distance.

7. Conclusion

The devices fabricated here demonstrate that transparent electrode membrane mirrors can produce large deformations (e.g. ±20 μm optical) at low spatial frequency, while under stable operation. This property makes them ideal for low order correctors in adaptive optics.

The requirement of stable device operation imposes constraints on the membrane-electrode gap distances and operating voltages. These constraints affect the range of possible deformations that can be imposed onto the membrane mirror by limiting the electrostatic pressure that may be applied, particularly as the spatial frequencies of the deformations are increased.

In particular, the magnitude of the transparent electrode bias voltage determines the maximum upward deformation that can be imposed on the membrane. Stability requires this voltage to be relatively low, and when this voltage is applied to individual actuators, or binned groups of actuators, e.g. to demonstrate an influence function, the resulting deformation will necessarily be only a fraction of the snap down distance.

Large deformations at high spatial frequency can be accomplished with devices made with larger gap distances operated at higher voltage than existing devices. For example, a device with 75 μm gap distance would generate 8.5 μm amplitude deformation for j=1 eigenfunction with 110 V electrode array operation. This same device would exhibit 2-3 μm peak deformation for higher order eigenmode deformations.

Together these simulations and experiments suggest that low stress membrane mirrors with gap distances in the 50-100 μm range can generate large, low order optical corrections and modest high order corrections with stable operation at moderate voltage.

---

[1] Robert Aldrich, in *Adaptive Optics Engineering Handbook*, edited by Robert Tyson (Marcel Dekker, New York, 2000), p.151-157.

[2] Gleb Vdovin and Paul M. Sarro, Applied Optics **34**, 2968-2972 (1995).

[3] Peter Kurczynski, Harold M. Dyson, Bernard Sadoulet, J. Eric Bower, Warren Y-C Lai, William M. Mansfield, and J. Ashley Taylor, MOEMS and Miniaturized Systems V, SPIE Vol 5719, 155, (2005), edited by Ayman El-Fatatry SPIE, Bellingham, WA, (2005).

[4] R. P. Grosso and M. Yellin, J. Opt. Sci. Am. **67**, 399 (1977).

5 P. Kurczynski, H.M. Dyson, B. Sadoulet, J.E. Bower, W. Y-C Lai, W. M. Mansfield, J. A. Taylor, "Fabrication and measurement of low-stress membrane mirrors for adaptive optics." Applied Optics Vol. 43 (18) 3573-3580, 2004.